ISSN 1330-3651 (Print), ISSN 1848-6339 (Online)
Received: 14 June 2025; Accepted: 19 November 2025

https://doi.org/10.17559/TV-20250614002748
Original scientific paper

Design and Analysis of a Dual Radial MIMO Implantable Antenna for WMTS Applications

N. SRIVIDHYA, P. MAHESWARA VENKATESH*

Abstract: This research presents a meticulously engineered dual-port, dual-radial implantable MIMO (Multiple Input Multiple Output) antenna specifically designed to operate within the 1.39-1.42 GHz frequency band of the Wireless Medical Telemetry System (WMTS). The proposed antenna, with compact dimensions of 19 × 19 × 1.27 mm³, utilizes Rogers RO6010 as both substrate and superstrate, featuring a dielectric constant (ε_r) of 10.2, a thickness of 0.635 mm, and a loss tangent of 0.0023. The design achieves high isolation (> 20 dB) between antenna elements, ensuring minimal mutual coupling, enhanced signal integrity, and reduced interference in implantable biomedical communication environments. The antenna demonstrates excellent performance metrics including a low Envelope Correlation Coefficient (ECC < 0.1), signifying robust signal decorrelation and high data reliability. Furthermore, the diversity gain (DG) approaches 10 dB, improving reception diversity and mitigating multipath and fading issues. Despite its compact and low-power design, the antenna achieves a peak gain of -28 dB and a measured channel capacity (CC) of 8 bps/Hz, indicating suitability for high-data-rate applications. Fabrication and measurement results exhibit strong agreement with simulated data, confirming the proposed antenna's practical feasibility for next-generation biomedical implant communication systems.

Keywords: biomedical telemetry; envelope correlation coefficient; implantable antenna; MIMO systems; wireless medical telemetry system (WMTS)

1 INTRODUCTION

Biomedical antennas are crucial for wireless communication, remote monitoring, implantable medical devices, wearable technology, telemedicine, and medical imaging. They enable enhanced patient care, personalized medicine, and advancements in medical technology, leading to improved healthcare outcomes and quality of life. Implantable antennas are vital for various biomedical science applications, especially regarding wireless and implanted medical technologies. Their unique characteristics make them ideal for use in implantable medical devices like pacemakers [1-3], neurostimulators [4], implantable drug delivery systems, retinal prosthesis [5], capsule endoscopy [6], choler implant and wireless biosensors [7]. A dual band, 2.4 and 4.8 GHz neuro-sensing device for wireless deep brain signal monitoring was presented by the authors in [8]. These characteristics ensure reliable communication, better signal reception, dual band applications [9], improved coverage, and minimized interference. Additionally, implantable antenna helps to reduce interference from external sources by attenuating or rejecting orthogonal linear polarized signals from nearby devices or ambient electromagnetic noise. This improves overall signal quality and decreases the risk of interference-related performance issues. Achieving circular polarization in antennas involves applying electromagnetic theory, antenna design principles, feeding techniques, and meticulous engineering considerations. In [10], authors describe an implantable MIMO antenna with a spiral form and a helix line grounded for use in wireless biotelemetry applications operating in the Med-Radio (401-406 MHz) frequencies. The high dielectric Rogers RT/duroid 6010 substrate, with relative permittivity $\varepsilon_r = 10.2$, tangential loss = 0.0023, and 25 mil thickness, was utilised to print the intended antenna, which has a footprint of $22 \times 22 \times 0.635$ mm^3. In [11], they looked into an implantable MIMO antenna with four elements that is cross-shaped and based on electroencephalography (EGB) for high-speed biological applications using the ISM band. The designed bio-implantable antenna has dimension foot print of $18.5 \times 18.5 \times 1.27$ mm^3. With the notion of MIMO, authors in [12] have developed a dual-band low profile implanted antenna. Applications for long-range, high-speed data transfer using scalp implantation and capsule endoscopy. A pair of rectangular and arc-shaped slots was placed over the defective ground construction and radiating patch in order to further reduce the entire size. In order to achieve improved transmission rates in deep implant biomedical components at the 2.45 GHz band, a meandering structure implantable antenna accessible in MIMO was used in [13].

Authors in [14], looked at the conformal helical shaped MIMO antenna for wireless neurostimulator applications. Through the use of fractal-shaped MIMO antenna, a broad fractional bandwidth of 37% was attained in [15]. With authors in [16], a semi-circular slotted dual band implantable antenna with peak gain, a decent reflection coefficient, and a respectable front to back ratio (FBR) range was accomplished. A major challenge in MIMO antenna design was to minimise mutual contact between antenna elements within the limited antenna system footprint. As far as the authors are aware, no quantitative study has been conducted on the MIMO technique for implantable applications, particularly on an implanted MIMO antenna with a dual radial stub fractal structure. In this paper, rectangular shaped dual slotted patch with full ground structure antenna was proposed for different dielectric permittivity of human brain, skin and heart implantable applications [17]. The proposed implantable antenna is compact and achieves a peak realized gain of -28.3 dBi at 1.42 GHz. Its dimensions are 19 mm × 19 mm × 1.27 mm. To simulate skin, fat, muscle, and cardiac qualities, a homogeneous triple layer phantom measuring 60 mm by 40 mm by 20 mm was utilised. The antenna was placed 4 mm below the top of the phantom. This paper is organized as follows. Section II consists of the proposed dual stub MIMO implantable antenna geometry structure evolution stages with its *S*-parameter analysis. Results from simulations and measurements are contrasted in section III. Through simulation, the effects of SAR are looked into, and it is discovered that it complies with IEEE requirements.

2 ANTENNA STRUCTURE AND DESIGN ANALYSIS

The geometry of the proposed antenna is illustrated in Fig. 1. The antenna employs a double radial stub-based fractal geometry arranged periodically in rows and columns within the aperture dimensions $L \times W$.

Structure Description

As shown in Fig. 1a, the radiating elements are distributed across the aperture in a periodic arrangement to form the active patch layer. Each element is realized using double radial stubs, optimized to achieve resonance at the biomedical frequency of interest. The entire antenna structure is fabricated on a Rogers RO6010 substrate, which provides a high dielectric constant ($\varepsilon_r = 6.15$) and a low loss tangent (0.0023), thereby ensuring compact size and stable operation within biological tissue environments. The overall substrate size is $19 \times 19 \times 0.635$ mm^3.

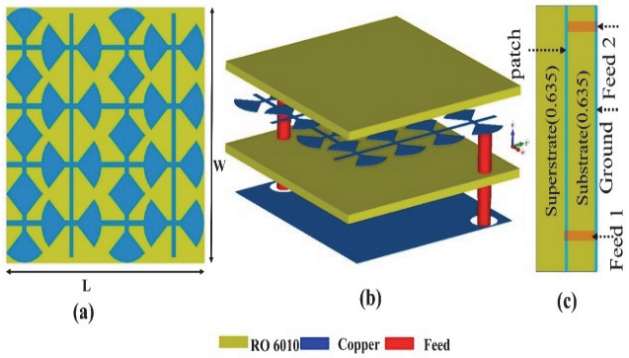

Figure 1 Design of implantable MIMO antenna: (a) Front view, (b) Isometric view, (c) Side view dimensions: *W*, *L* =19 (unit: mm)

The 3D view in Fig. 1b shows that the antenna is composed of three layers:

1. Patch layer - consisting of the periodic double radial stub arrangement.
2. Ground plane - positioned beneath the substrate to confine backward radiation.
3. Superstrate layer - an additional RO6010 sheet of thickness 0.635 mm placed above the patch.

The use of the superstrate layer serves two purposes: (i) to further miniaturize the antenna profile, and (ii) to improve 50-Ω impedance matching by reducing detuning effects caused by tissue loading.

The cross-sectional view of the antenna is shown in Fig. 1c. It highlights the substrate-patch-superstrate stack-up, along with two coaxial probe feeds. Feed 1 and Feed 2 are connected at diagonally opposite locations of the patch layer, enabling dual-port excitation for MIMO operation. The coaxial probe has a 50-Ω characteristic impedance, ensuring efficient power transfer.

To provide clarity in the design methodology, the stepwise evolution of the antenna is presented in Fig. 2.

Stage I & II: The design begins with a double radial stub configuration having dimensions $L_{1,2} = 4$ mm, $W_{2,3} =$ 0.3,1 mm, and $\theta = 90°$. This stage establishes the basic radiator geometry capable of supporting resonance in the desired frequency range.

Stage III: In this stage, multiple radial stubs are interconnected with curved sections of thickness 0.3 mm, arranged in rows and columns within the overall $L \times W$ aperture. This interconnection enhances current distribution uniformity and improves impedance matching. The fractal-inspired evolution contributes to size reduction while maintaining wideband characteristics.

Stage IV: The final geometry is obtained by rotating the radial stub by 90°, which further optimizes the reflection coefficient at the target resonance frequency. At this stage, a dual-port configuration is introduced across the diagonals to enable MIMO operation. The final structure, composed of several unit cells, results in the proposed antenna array shown in Fig. 2.

The proposed antenna was simulated using CST Microwave Studio Suite within a three-layer human phantom model (dimensions: $60 \times 40 \times 20$ mm^3) to replicate realistic biomedical conditions. The antenna's performance is influenced by implantation depth, as deeper placement may cause detuning and reduced efficiency. However, for typical biomedical applications such as pacemakers and biotelemetry devices, which generally require shallow-to-moderate implantation, the proposed design maintains reliable operation. The antenna was implanted 4 mm deep into human muscle tissue, and evaluations were further conducted in pork tissue to validate the simulation results.

The reflection coefficient characteristics are presented in Fig. 2, where the antenna resonates at 1.4 GHz with S11 less than -10 dB, indicating satisfactory impedance matching. The achieved bandwidth is approximately 172 MHz, which is sufficient for biotelemetry and implantable medical device communication. The transmission coefficient analysis of the dual-port structure reveals an isolation level greater than 20 dB, demonstrating the suitability of the design for MIMO applications.

$L_{1,2} = 4$ mm, $W_{2,3} = 0.3$, 1 mm and $\theta = 90°$

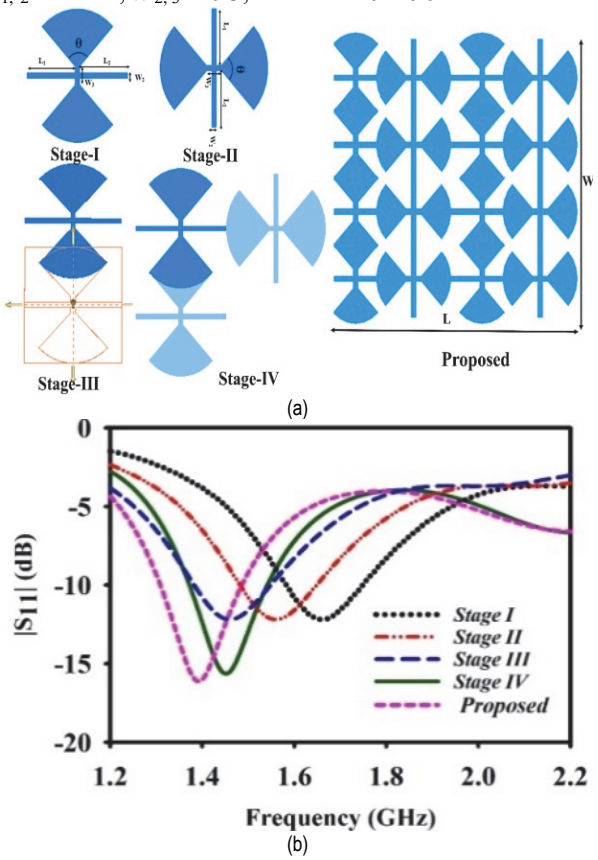

Figure 2 Design stages of proposed antenna: (a) Radial stub MIMO antenna element, (b) *S*-parameter analysis

As implantable antennas operate in close proximity to biological tissues, it is essential to evaluate their Specific Absorption Rate (SAR). The proposed antenna was analyzed for SAR at 1.4 GHz, considering the tissue-loading effects.

The choice of the 1.39-1.42 GHz WMTS band is significant because it is officially reserved for medical use by regulatory bodies such as the FCC. Unlike unlicensed ISM bands, this spectrum is not shared with consumer devices like Wi-Fi, Bluetooth, or RFID, thereby reducing the risk of interference. As a result, it ensures reliable communication, improves patient safety, and meets healthcare communication standards, making it well suited for implantable and body-centric medical devices.

3 RESULTS AND DISCUSSION

The suggested two-element antenna has been fabricated, and its performance has been thoroughly evaluated. The full-wave electromagnetic simulations of the proposed implantable antenna were carried out using CST Microwave Studio 2023. The Finite Integration Technique (FIT)-based frequency domain solver was employed for all analyses. A hexahedral adaptive mesh was applied, with a minimum mesh step size of approximately $\lambda/40$ at the highest simulated frequency to ensure numerical accuracy. The adaptive meshing was continued until the *S*-parameter convergence was better than 0.01 dB between iterations. Open (add space) boundary conditions were used in all directions to emulate free-space radiation, and waveguide ports were assigned for excitation. The antenna model was placed inside a homogeneous multilayer tissue-equivalent phantom for bio-medical analysis.

For experimental validation, the designed antenna was placed inside a 60 × 40 × 20 mm³ tissue-equivalent homogeneous Bio/skin phantom, as illustrated in Fig. 3a. This phantom replicates the layered structure of skin, fat, and muscle, thereby providing a realistic approximation of the implant operating environment. Such a model is widely used in biomedical antenna studies because it mimics the dielectric properties of human tissues, enabling accurate assessment of antenna behavior under realistic conditions.

The constructed prototype, imprinted on a 0.635 mm-thick substrate, is shown in Fig. 3b. *S*-parameters were assessed utilizing Keysight's network analyser, with port 1 serving as the testing port and port 2 being terminated by a 50-Ω terminator. The proposed antenna's measurement setup with the minced pork meat is shown in Fig. 3c. Notably, over the desired operating frequency, the measured values agree quite well with the simulation results. Furthermore, the radiation characteristics of the designed antenna placed in the anechoic chamber and observed; its pattern is shown in Fig. 3d.

The resultant reflection coefficient performance is presented in Fig. 4a and co and cross polarisation representations of measured and simulated radiation patterns in free space are shown in Fig. 4b. The antenna radiates in both directions at 1.4 GHz, and its cross polarisation is significantly less than -50 dB. The results of the simulation and measurement accord well with one another. At 1.4 GHz, the simulated realised gain is -27 dBi. As illustrated in Fig. 4b, the measured findings, however, reveal a realised gain of -28 dB.

A particular mathematical expression, as in Eq. (1), can be used to calculate the possible data transmission capacity in a typical MIMO communication arrangement.

$$\text{ChannelCapacity} = N\log_2\left(1+\frac{A}{B}\right)\left(1-C_{12}\right) \tag{1}$$

where, N = number of elements, A = Signal Power, B = Noise Power, and C = ECC.

This formula takes into account variables like the correlation coefficient between each individual antenna in the system and the degree of noise. Within this framework, the proposed antenna elements' data transfer capability (within a single-band module) was determined assuming no correlation between transmitting antennas. Additionally, the analysis was predicated on the transmitting and receiving antennas being in a Rayleigh fading environment with a 20 dB signal-to-noise ratio (SNR) and having links that linked them with the same distribution patterns. Fig. 5a displays the data transfer capability of the suggested antenna design as represented graphically by the simulation results. In order to establish the context, the ideal data capacity of a single-input-single-output (*zz*) setup is also displayed for comparison.

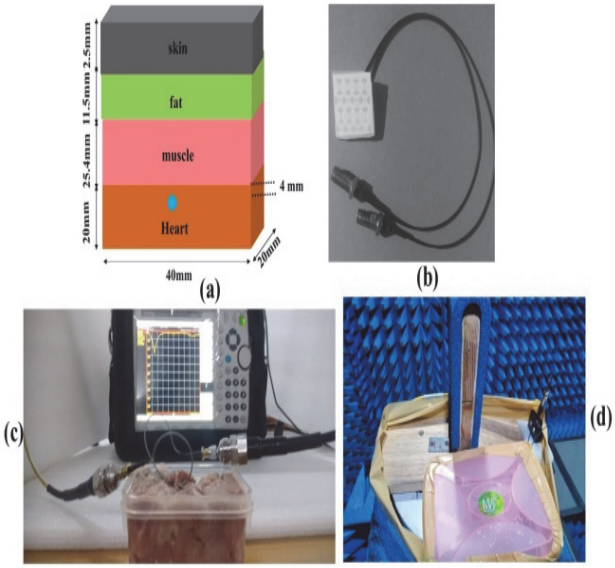

Figure 3 (a) Homogeneous three-layer phantom with its dimensions, (b) Protype of the antenna, (c) *S*-parameter measurement in minced pork meat, (d) Radiation pattern measurement setup

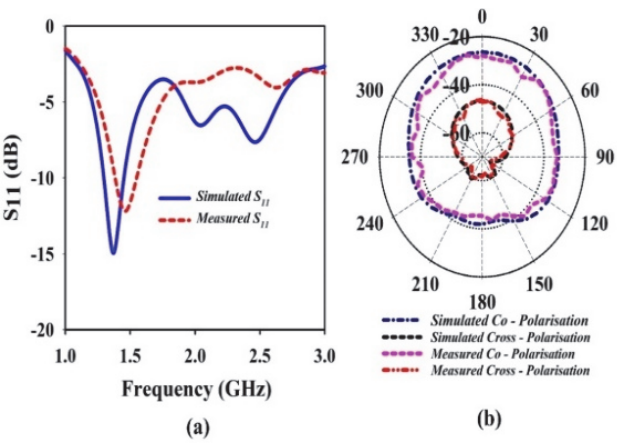

Figure 4 (a) Reflection Coefficient Analysis, (b) Pattern of far-field emission of the proposed antenna at 1.4 GHz

As illustrated in Fig. 5a, the computed data transmission capacity for the recommended single-band module elements is 8 bits per second per Hertz (bps/Hz) over a bandwidth of 1.4 GHz.

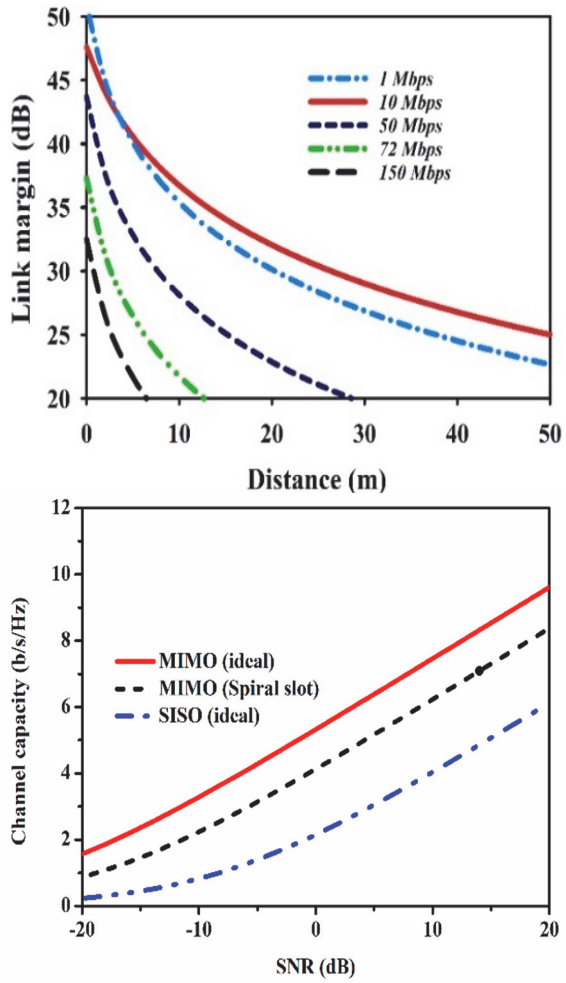

Figure 5 (a) Calculated channel capacity, (b) Link margin of the proposed antenna

As seen in Fig. 5a, the signal to noise ratio (SNR) has been adjusted from -20 to 20 dB to give clarity over the channel capacity. It is evident that the MIMO system performs better in terms of channel capacity the higher the SNR value. The proposed MIMO, SISO, and MIMO under ideal conditions are plotted against SNR (dB) in Fig. 5a. The proposed MIMO implantable antenna surpasses an ideal SISO (CC = 6.12 bps/Hz) with a CC of 8.37 bps/Hz at SNR = 20 dB.

One important parameter in wireless implantable communication systems is the Link Margin (LM), which is expressed in db. It represents the difference between the least power that is predicted to reach the receiver and the receiver's sensitivity threshold, or the point at which the receiver stops working. When the system has a 15 dB link margin, it means that it can withstand an extra 15 dB of signal deterioration between the transmitter and the receiver while still operating at maximum efficiency.

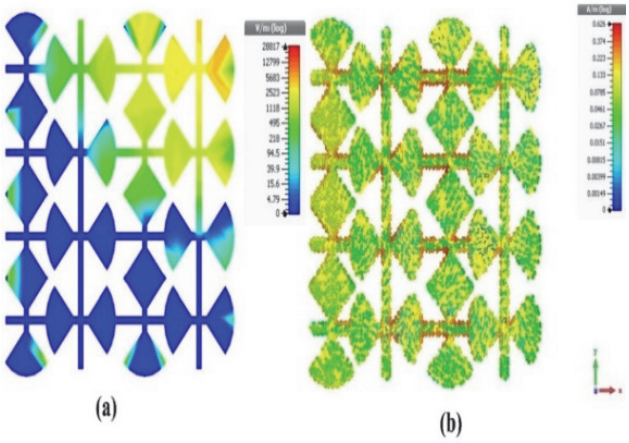

Figure 6 E-field and current distribution of the MIMO antenna: (a) E-field strength and (b) Surface current at radial stub

Table 1 Performance comparison of the designed antenna with other antennas presented in the literature

Reference. year		[16] 2018	[13] 2021	[18] 2021	[20] 2022	[19] 2022	Proposed
Antenna Configuration (MIMO)		Band gap	Meander	Slot	Spiral	Radiating strip	Radial stub
Designed Frequency / GHz		2.45	0.4	2.41	2.45	0.403,0.433	1.4
Volume / mm^3		434	127	280	3.98	13	229
Dimensions / mm		18.5 × 18.5 × 1.27	10 × 10 × 1.27	20 × 22 × 1.27	5.3 × 6.2 × 0.12	12 × 11 × 1.27	19 × 19 × 1.27
Ports		4	4	2	2	2	2
Dielectric material		RT duroid 6010	RT duroid 3010	RT duroid 6010	RT duroid 3010	RT duroid 3010	RT duroid 6010
S-parameter $\|S_{11}\|$ / dB		-12	-25	-15	-30	-20	-17
BW ($\|S_{11}\| < -10$ dB)		18.64	38.6	8.5	28	33.9	12.76
SAR / W/Kg	1 g	342	326	66.5	562	486	406
	10 g	860	543	347	402.8	538	47.3
ECC		0.12	0.16	Less than 0.1	Less than 0.1	0.15	0.12
Maximum gain / dB		-15.8	-27.2	-22.3	-20.5	-30	-28.3

The distribution of surface current and E-field on the radiating radial stub is shown in Fig. 6a and Fig 6b. At the point of port near radial stubs, a strong E-field density is detected. Furthermore, as noted in the Fig. 6b legend, the surface current flow across the radiating radial stub element was obtained to be 0.6 m/A.

SAR Analysis

Simulated SAR values at 1.4 GHz for 1-gram and 10-gram average tissue standards are presented using a 3-layer phantom model. The SAR values of 406 W/kg and 47.3 W/kg respectively for 1-gram and 10-gram average tissue standards are shown in Fig. 7.

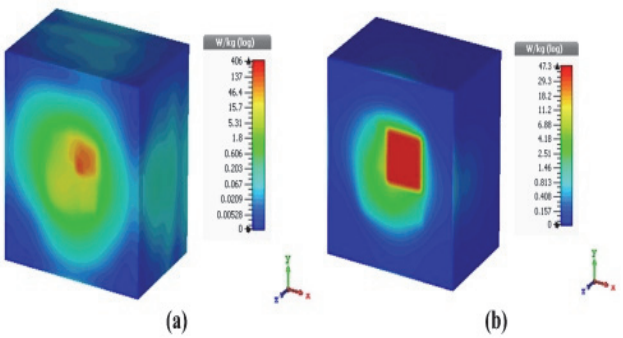

Figure 7 SAR estimation of the proposed bio-medical antenna: (a) 1-gram standard and (b) 10-gram standard

Fig. 7 illustrates how well the suggested antenna performs when placed inside human skin, such as in an acidic environment. It is noted that the presence of human tissue, such as a solution, has no effect on antenna performance. The evaluation of electromagnetic radiation health concerns is based on the Specific Absorption Rate (SAR), which is calculated using Eq. (2) and Eq. (3).

$$\text{SpecificAbsorptionRate(SAR)} = \frac{\sigma \left| E^2 \right|}{\rho} \tag{2}$$

$$\text{Power} = \frac{E \frac{v^2}{m^2}}{120\pi} w/m^2 \tag{3}$$

Fig. 5b illustrates that the connection margin gets stronger with increasing transmitter-to-receiver distance and gets worse with decreasing transmitter-to-receiver distance.

The simulated SAR values at 1.4 GHz were found to be 406 W/kg for the 1-g average and 47.3 W/kg for the 10-g average. These values exceed the safety thresholds specified by international standards, namely 1.6 W/kg for 1 g (IEEE/FCC) and 2.0 W/kg for 10 g (ICNIRP).

The elevated SAR results are primarily due to the small dimensions of the tissue-equivalent phantom (60 × 40 × 20 mm³), which concentrate the absorbed power into a limited volume, and the higher excitation power level used during simulation. In practical implantable scenarios, the input power is significantly lower (typically 0.25-1 mW for medical telemetry devices), and SAR scales linearly with the input power. For example, reducing the excitation power from 1 W in simulation to 1 mW in practice would decrease the SAR by a factor of 1000, yielding values of approximately 0.406 W/kg (1 g) and 0.047 W/kg (10 g), which are well below the IEEE/ICNIRP limits. Similar observations regarding the overestimation of SAR in scaled-down phantoms and the subsequent reduction under realistic power levels have been reported in previous implant antenna studies [19]. Thus, the proposed antenna can be considered safe for biomedical applications when operated under practical conditions.

MIMO Parameters

This section looks at the intended antenna's key MIMO channel parameters, such as Envelope Correlation Coefficient (ECC), Channel Capacity (CC), and Diversity Gain (DG).

One of the crucial MIMO parameters is the ECC. It can be computed using the far field results or the S parameter. One way to compute the ECC is as follows:

$$\text{ECC} = \frac{\left| S^*_{11} S_{12} + S^*_{21} S_{22} \right|^2}{\left(1 - \left|S_{11}\right|^2 - \left|S_{21}\right|^2\right)\left(1 - \left|S_{12}\right|^2 - \left|S_{22}\right|^2\right)} \tag{4}$$

For the entire resonance frequency, an ECC less than 0.5 is considered a satisfactory result; exceptionally high ECC value validates the outstanding diversity performance.

However, the simulated ECC for the skin values is less than 0.1 in the ISM band, as shown in Fig. 8. Similar to ECC, DG is a crucial indicator that has an inverse relationship with the assessment of MIMO systems.

$$\text{DG} = 10\sqrt{\left(1 - \text{ECC}^2\right)} \tag{5}$$

Perfectly coupled MIMO channels are expected to have a DG of 10 dB. As seen in Fig. 8, the simulated DG is higher than 9.98 dB. Without requiring extra power or frequency spectrum resources, high data rate transmission is made possible. A lot of people know that when a MIMO has more antennas inside, its channel capacity improves. However, this is only true for uncorrelated channels; with correlated channels, less mutual coupling is needed.

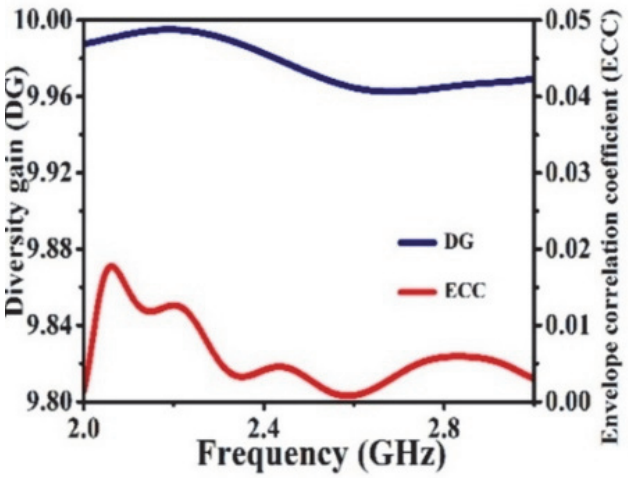

Figure 8 ECC and DG of the designed radial stub implantable antenna

For reliable MIMO performance, an ECC value below 0.5 is generally considered acceptable [1, 3, 12, 15-16]. In the proposed design, the simulated ECC is consistently below 0.1 across the ISM band (Fig. 8), which indicates very low correlation between antenna elements and hence excellent spatial diversity. Such a low ECC is highly favorable for biomedical implants, as it ensures robust communication even in multipath-rich body-centric environments.

The corresponding DG values remain above 9.98 dB, approaching the theoretical maximum of 10 dB. This confirms that the proposed antenna can achieve maximum diversity performance, which is essential for minimizing fading effects and ensuring stable data links in wireless implant communications.

Channel capacity, another critical performance indicator, is observed to reach 8 bps/Hz, which is significantly higher than the typical capacity reported for compact implantable MIMO antennas [18-19]. This improvement demonstrates the antenna's ability to support high data rate wireless telemetry without requiring additional bandwidth or transmit power, an important factor for real-time biomedical data transfer, such as continuous ECG or EEG monitoring.

Thus, the combined results of ECC, DG, and channel capacity highlight the antenna's strong suitability for practical biomedical telemetry systems, offering low correlation, high diversity gain, and efficient spectrum utilization compared with earlier designs (Tab. 1).

As summarized in Tab. 1, the proposed antenna demonstrates clear advantages over earlier designs, particularly in terms of reduced size, broader operational bandwidth, lower SAR, and superior isolation. While some previous works report higher gain values, this often comes at the expense of larger geometries or narrower bandwidths. The present design strikes a balance by ensuring compactness and compliance with safety requirements, making it highly suitable for implantable biomedical applications.

4 CONCLUSION

In conclusion, a significant advancement in antenna engineering has been demonstrated through the design and analysis of a dual-port antenna operating within the 1.39-1.42 GHz ISM frequency band. By adhering strictly to the design parameters, a highly efficient implantable antenna with excellent isolation, reliability, and overall performance has been achieved. The antenna exhibits more than 20 dB isolation between ports, ensuring enhanced signal integrity in complex communication environments. Furthermore, its outstanding efficiency supports optimal power utilization without compromising performance. The measured results confirm a channel capacity of 8 bps/Hz, low envelope correlation coefficient (ECC), and a diversity gain of approximately 10 dB, making the antenna a strong candidate for high-data-rate wireless communication systems. The close agreement between simulation and experimental measurements validates the proposed design and reinforces its suitability for real-world deployment in diverse applications, including telecommunications, IoT devices, and high-speed data transfer.

Overall, this work provides both a solid theoretical foundation and practical verification of an effective implantable dual-port antenna, thereby paving the way for further advancements in modern wireless and biomedical communication technologies.

5 REFERENCES

[1] Zada, M., Shah, I. A., Basir, A., & Yoo, H. (2021). Ultra-Compact Implantable Antenna with Enhanced Performance for Leadless Cardiac Pacemaker System. *IEEE Transactions on Antennas and Propagation*, *69*(2), 1152-1157. https://doi.org/10.1109/TAP.2020.3008070

[2] Ganesan, R., Panchavarnam, M. V., & Thangaiyan, J. (2023). Split Ring Resonator Inspired Dual-Band Monopole Antenna for ISM, WLAN, WIFI, and WiMAX Application. *Tehnički vjesnik*, *30*(5), 1533-1538. https://doi.org/10.17559/TV-20230210000344

[3] Faisal, F., Zada, M., Yoo, H., Mabrouk, I. B., Chaker, M., & Djerafi, T. (2022). An Ultra-miniaturized Antenna with Ultra-wide Bandwidth for Future Cardiac Leadless Pacemaker. *IEEE Transactions on Antennas and Propagation*, *70*(7), 5923-5928. https://doi.org/10.1109/TAP.2022.3161513

[4] Orhan, A. & Mesud, K. (2022). The Effect of the Co-Planar Structure on HPBW and the Directional Gain at the Square Patch Antenna around ISM 2450 MHz. *Technical Gazette*, *29*(4), 1120-1125. https://doi.org/10.17559/TV-20190423010908

[5] Feng, Y. & Li, Y. (2020). Design and System Verification of Reconfigurable Matching Circuits for Implantable Antennas in Tissues With Broad Permittivity Range. *IEEE Transactions on Antennas and Propagation*, *68*(6), 4955. https://doi.org/10.1109/TAP.2019.2955291

[6] Kangeyan, R. & Karthikeyan, M. (2023). Implantable Dual Band Semi-Circular Slotted Patch with DGS Antenna for Biotelemetry Applications. *Microwave and Optical Technology Letters*, *65*(1), 225-230. https://doi.org/10.1002/mop.33462

[7] Lee, S. H. et al. (2011). A Wideband Spiral Antenna for Ingestible Capsule Endoscope Systems: Experimental Results in a Human Phantom and a Pig. *IEEE Transactions on Biomedical Engineering*, *58*(6), 1734-1741. https://doi.org/10.1109/TBME.2011.2116018

[8] Liu, C., Guo, Y. X., & Xiao, S. (2014). Circularly Polarized Helical Antenna for ISM-Band Ingestible Capsule Endoscope Systems. *IEEE Transactions on Antennas and Propagation*, *62*(12), 6027-6039. https://doi.org/10.1109/TAP.2014.2364074

[9] Bao, Z. & Guo, Y.-X. (2017). Single-Layer Dual-/Tri-Band Inverted-F Antennas for Conformal Capsule Type of Applications. *IEEE Transactions on Antennas and Propagation*, *65*(12), 6400-6405. https://doi.org/10.1109/TAP.2017.2758161

[10] Li, R. & Guo, Y. (2021). A Conformal UWB Dual-Polarized Antenna for Wireless Capsule Endoscope Systems. *IEEE Antennas and Wireless Propagation Letters*, *20*(4), 483. https://doi.org/10.1109/LAWP.2021.3054676

[11] Chen, W.-C. & Lee, C. W. L. (2018). A Multi-Channel Passive Brain Implant for Wireless Neuropotential Monitoring. *IEEE Journal of Electromagnetics, RF, and Microwaves in Medicine and Biology*, *2*(4), 242-249. https://doi.org/10.1109/JERM.2018.2877330

[12] Kangeyan, R. & Karthikeyan, M. (2023). Miniaturized Meander-Line Dual-Band Implantable Antenna for Biotelemetry Applications. *ETRI Journal*, *2023*, 1-8. https://doi.org/10.4218/etrij.2023-0050

[13] Liu, C., Li, Y., Yang, X. M., & Liu, X. (2016). Small-Size Dual-Antenna Implantable System for Biotelemetry Devices. *IEEE Antennas and Wireless Propagation Letters*, *15*, 1723-1726. https://doi.org/10.1109/LAWP.2016.2528987

[14] Fan, Y., Huang, J., Chang, T., & Liu, X. (2018). A Miniaturized Four-Element MIMO Antenna with EBG for Implantable Medical Devices. *IEEE Journal of Electromagnetics, RF and Microwaves in Medicine and Biology*, *2*(3), 226-233. https://doi.org/10.1109/JERM.2018.2871458

[15] Iqbal, A., Al-Hasan, M., Mabrouk, I. B., & Nedil, M. (2022). A Compact Implantable High-Data-Rate Biotelemetry Applications. *IEEE Transactions on Antennas and Propagation*, *70*(1), 631-640. https://doi.org/10.1109/TAP.2021.3098606

[16] Alazemi, A. J. & Iqbal, A. (2022). A High Data Rate Implantable MIMO Antenna for Deep Implanted Biomedical Devices. *IEEE Transactions on Antennas and Propagation*, *70*(2), 998-1007. https://doi.org/10.1109/TAP.2021.3111186

[17] Kangeyan, R. & Karthikeyan, M. (2023). A Novel Wideband Fractal-Shaped MIMO Antenna for Brain and Skin

Implantable Applications. *International Journal of Communication Systems*, *36*(11) e5509. https://doi.org/10.1002/dac.5509

[18] Alazemi, A. J., Iqbal, A., Smida, A., Ghayoula, R., Mallat, N. K., Kim, S., & Kim, D. I. (2022). A compact and wideband MIMO antenna for high-data-rate implantable communications. *Scientific Reports*, *12*(1), 14290. https://doi.org/10.1038/s41598-022-18468-2

[19] Kiani, S. H., Iqbal, A., Basir, A., Al-Hasan, M., Mabrouk, I., & Denidni, T. A. (2025). A Compact Multi-Channel Implantable Antenna for High-Speed Telemetry. *IEEE Transactions on Antennas*, *73*(8) 5209-5216. https://doi.org/10.1109/TAP.2025.3564738

Contact information:

N. SRIVIDHYA
Department of Electronics and Communication Engineering,
K. Ramakrishnan College of Engineering,
Trichy, Tamil Nadu, India
E-mail: srividhyanagamuthu@gmail.com

P. MAHESWARA VENKATESH, Assistant Professor (SI.Gr)
(Corresponding Author)
Department of Electronics and Communication Engineering,
University College of Engineering, BIT Campus, Anna University, Tiruchirappalli
E-mail: maheshwaravenkatesh@gmail.com